Journal of Marine Science and Technology

Volume 31 | Issue 4 Article 10

Research On Ice Resistance Of Ships Sailing In Floating Ice Floe

Zhixin Xiong
College of Ocean Science and Engineering, Shanghai Maritime University, Shanghai 201306, China

Xinyuan Wu
College of Ocean Science and Engineering, Shanghai Maritime University, Shanghai 201306, China, 1427103043@qq.com

Yang Li
China Offshore Engineering & Technology Co,. Ltd., Shanghai 200001, China

Recommended Citation

Xiong, Zhixin; Wu, Xinyuan; and Li, Yang (2023) "Research On Ice Resistance Of Ships Sailing In Floating Ice Floe," *Journal of Marine Science and Technology*: Vol. 31: Iss. 4, Article 10.
DOI: 10.51400/2709-6998.2717
Available at: https://jmstt.ntou.edu.tw/journal/vol31/iss4/10

RESEARCH ARTICLE

Research on Ice Resistance of Ships Sailing in Floating Ice Floes

ZhixinXiong [a], Xinyuan Wu [a,*], Yang Li [b]

[a] College of Ocean Science and Engineering, Shanghai Maritime University, Shanghai 201306, China
[b] China Offshore Engineering & Technology Co, Ltd., Shanghai 200001, China

Abstract

To study the ice resistance of ships in areas with floating ice, the *Xuelong 2* icebreaker was simulated. A floating-ice model was established using the discrete-element method, and an ice particle array was generated using MATLAB. The effects of ice coverage and speed on ice drag were studied From the numerical simulation results, it can be seen that there is a certain trend in ice resistance under different ice coverage ranges, which changes with the change of speed. By comparing with the empirical formula and the numerical value of the ship model test, this numerical simulation results are relatively accurate. It also provides a reference for evaluating the ice resistance of Xuelong 2 in the floating ice area.

Keywords: Ice resistance, Floating ice floes, Ice coverage

The exploitation of polar resources and waterways has attracted substantial attention in recent years. Notably, the development of polar waterways for international shipping has resulted in the increased use of icebreakers. The resistance caused by level and floating ice floes during the navigation of icebreakers in polar areas must be considered during ship design and development [1]. Global warming has induced a paradigm change in the arctic environment because of the transition from level ice coverage to broken ice floes and open water fields [2]. This navigation environment considerably affects ships; level ice coverage does not become open water but instead becomes numerous ice floes that float on the sea surface [3]. These ice floes tend to be circular because of the effects of wave wash and floe−floe collisions. In the event of a collision between a ship and an ice floe, the hull and floating ice might be crushed and damaged. If the crushing force reaches a critical level, radial cracks form in large pieces of floating ice, which results in them decomposing into multiple small pieces of ice that accumulate on the ship's hull [5]. These ice floe fields are predominantly found in the Antarctic along routes that are common shipping paths [2,4]. Studies have indicated that vessels navigating in floe waters experience substantial ship resistance. To address this problem, researchers have investigated and predicted ice-induced ship resistance through research ship expeditions and simulations with real data [3]. Some research expedition vessels employed for such studies include *Xuelong 2*, *Icebreaker Oden*, and *Icebreaker Polarstern*.

In the floating-ice environment, the density of the ice varies, which affects the frequency at which ships collide with the floating ice. Simulating ship−ice interactions can be complex because the large displacement of hulls, ice fracturing and fragmenting, and the motions of the ice fragments must be considered [6]. Numerical methods are essential for optimizing the design of ice-going vessels because model tests are prohibitively expensive and time-consuming. The discrete-element method (DEM), which is a numerical simulation method, is a key approach for analyzing

Received 6 May 2023; revised 22 October 2023; accepted 31 October 2023.
Available online 15 December 2023

* Corresponding author.
E-mail address: 1427103043@qq.com (X. Wu).

https://doi.org/10.51400/2709-6998.2717

ship−ice interactions. It can be used to not only simulate the ice structure at the microscopic scale but also simulate ice breakup at the macroscopic scale. Therefore, the DEM has been widely used for numerical simulations of ice resistance in floes because this method is effective for modeling and analyzing the dynamic characteristics of floating ice and crushed ice and can provide a reference for determining ship navigation methods in fields of floating large and small ice floes [7,8].

The DEM was first proposed by academician Peter Cundall in the early 1970s for solving dynamic problems of discrete systems [9]. Fundamentally, the DEM involves discretizing a medium into numerous individual units that have certain physical and geometric characteristics (such as shape, size, and distribution) [10]. The contact or separation between each unit is defined, and relationships between movement, contact, and energy conversion are determined. The motion of a single discrete element is controlled by the classical equations of motion, and the motion and deformation of the entire medium ultimately depend on the motion and displacement of each element [11]. The DEM was initially applied in the field of geomechanics to study the mechanical behavior of discontinuous media, such as rocks. Over the last 50 years, the DEM has been widely used in mineral engineering, civil engineering, chemical engineering, and other fields [12].

Hansen and Løsetb [13] used the DEM with two-dimensional disk elements to calculate the hull ice load for broken ice fields. Karulin [14] simulated interactions of cake ice with moored ships at different speeds and compared the results with those of a model test. Lau [15] used the three-dimensional discrete-element software DECICE to simulate the icebreaking ability and maneuverability of ships. Konno [13] used block units to explore the ice resistance of ships during sailing. Kim [16] improved an existing empirical formula by replacing the empirical coefficients with values calculated for specific ship types to calculate the icebreaking resistance, ice clearing resistance, and buoyancy resistance of the corresponding ship. Moon-Chan [17] used the LS-Dyna software program for numerically simulating ice resistance performance in a floating-ice environment and compared their results with model test data. They also discussed the effect of the speed of a ship on its ice resistance performance.

Jeong-Hwan Kim et al. produced a database from measured ice resistance data for 220 icebreakers with different characteristics to develop a data-driven ice resistance estimation method involving the use of an artificial neural network [18]. If various ship parameters were input to the network, it output the predicted ice resistance. In [19,20], the performance of sphere-based DEM and dilated-polyhedron-based DEM for analyzing ship−ice interactions was compared.

"Xuelong 2" is the world's first polar scientific expedition icebreaker with bow and stern bidirectional icebreaking technology. There have been several studies conducted on "Xuelong 2". For example, the polar application of the "Xuelong 2″ long column sampler [21] and the design and application of the lunar pool system of the "Xuelong 2″ polar exploration ship [22]. However, there are few literature investigating the floating ice resistance of the icebreaker "Xuelong 2" by CFD-DEM. The study focuses on boat and ice interactions and differs from the existing literature. Addressing this gap, our research focuses on ice resistance of "Xuelong 2" icebreaker in floating ice area through numerical simulation based on CFD-DEM analytical model. In view of this gap, the ice resistance of the "Xuelong 2" Icebreaker in the floating ice area was studied by numerical simulation based on the CFD-DEM analysis model, and by creatively controlling the ice floe converge. CFD method is used to assess the fluid solutions of the vessel (thus, the wake and water resistance of a ship). DEM method is employed to investigate ice floes and their collision with vessels; those floes obtain fluid force from the CFD solution so that the ship-wave-ice coupling is achieved [23−25].

First, the ship−ice model is discussed. Subsequently, the numerical calculations, an analysis of the results, and the conclusions are presented.

1. CFD-DEM coupling model

1.1. Discrete element method control equation

In addition to the STAR-CCM + software program, a DEM involving computational fluid dynamics was used to analyse the interaction between ships and floating ice. In general, ice floes should constantly satisfy Newton's second law of motion [26,27]. The following are the equations of motion under the actions of force and moment:

$$m_i \frac{dv_i}{dt} = \sum_j F_{ij} + F_g + F_{fluid} \tag{1}$$

$$\frac{d}{dt} I_i \omega_i = \sum_j T_{ij} \tag{2}$$

where v_i is the speed of floating ice i, F_{ij} is the noncontact force between floating ice i and floating ice j or other pieces of floating ice, F_g is the weight of

the floating ice, F_{fluid} is the fluid force, I_i is the rotational inertia of floating ice i, ω_i is the angular velocity of floating ice i, and T_{ij} is the contact moment acting on floating ice i because of a contact force other than floating-ice gravity.

1.2. Fluid particle interaction

In STAR-CCM+, a spring−damper system is used to calculate the contact force. In this calculation, overlaps between the particles and the wall are allowed, and an elastic force is generated by the spring. The contact force between the particles is represented as follows:

$$F_{\text{contact}} = F_{\text{n}} + F_{\text{t}} \tag{3}$$

where F_n is the normal force of contact between two floating-ice particles and F_t is the tangential force of contact between these particles.

A linear spring−damper contact model is used as the contact model in this study. The following equations express the normal component Fn and tangential component Ft of the contact force Fcontact:

$$F_{\text{n}} = -\text{k}_{\text{n}}\text{d}_{\text{n}} - \eta_{\text{n}}\text{v}_{\text{n}} \tag{4}$$

$$F_{\text{t}} = \begin{cases} -\text{k}_{\text{t}}\text{d}_{\text{t}} - \eta_{\text{t}}\text{v}_{\text{t}} \ , \ \text{if}|\text{d}_{\text{t}}| < |\text{d}_{\text{n}}|C_{\text{f}} \\ |\text{k}_{\text{n}}\text{d}_{\text{n}}|C_{\text{f}} \cdot \text{n} \ , \ \text{if}|\text{d}_{\text{t}}| \geq |\text{d}_{\text{n}}|C_{\text{f}} \end{cases} \tag{5}$$

where k is the modulus of elasticity; η represents damping, which is the energy consumed by the contact between particles; d_{n} and d_{t} are the overlap distances in the normal and tangential directions, respectively; V_{n} and V_{t} are the normal and tangential components, respectively, of the relative velocity between two contact particles; C_{f} is the friction coefficient, which is set as 0.35 between ice particles and 0.05 between the hull and ice particles [28]; k_{n} is the normal spring stiffness; k_{t} is the tangential spring stiffness; η_{n} represents the normal damping; and η_{t} represents the tangential damping.

$$\eta_{\text{n}} = 2\eta_{\text{ndamp}}\sqrt{\text{k}_{\text{n}}M_{eq}} \tag{6}$$

$$\eta_{\text{t}} = 2\eta_{\text{tdamp}}\sqrt{\text{k}_{\text{t}}M_{eq}} \tag{7}$$

$$M_{eq} = \frac{1}{\frac{1}{M_A} + \frac{1}{M_B}} \tag{8}$$

In the aforementioned equations, ηndamp is the normal damping coefficient, ηtdamp is the tangential damping coefficient, Meq is the equivalent mass of floating-ice particles, and MA and MB are the equivalent masses of floating-ice contact particles A and B, respectively.

The contact force between solid ice particles and dry, rigid, and unbreakable hulls is described by the Hertz−Mindlin contact model as follows [29]:

$$\text{k}_{\text{n}} = \frac{4}{3}E_{\text{eq}}\sqrt{R_{\text{eq}}\delta_{\max}} \tag{9}$$

$$\text{k}_{\text{t}} = 8G_{\text{eq}}\sqrt{R_{\text{eq}}\delta_{\max}} \tag{10}$$

$$E_{\text{eq}} = \frac{1}{\frac{1-\text{v}_A{}^2}{E_A} + \frac{1-\text{v}_B{}^2}{E_B}} \tag{11}$$

$$R_{\text{eq}} = \frac{1}{\frac{1}{R_A} + \frac{1}{R_B}} \tag{12}$$

$$G_{\text{eq}} = \frac{1}{\frac{2(2-\text{v}_A)(1+\text{v}_A)}{E_A} + \frac{2(2-\text{v}_B)(1+\text{v}_B)}{E_B}} \tag{13}$$

where $\delta_{\max}$ is the maximum overlap distance; E_{eq} is the equivalent Young's modulus; v_{A} and v_{B} are Poisson's ratios of particles A and B, respectively; E_{A} and E_{B} are Young's moduli of particles A and B, respectively; R_{eq} is the equivalent radius; R_{A} and R_{B} are the radii of particles A and B, respectively; and G_{eq} is the equivalent shear modulus.

For collisions between particles and walls, the wall radius can be assumed to be Rwall = ∞, with the wall mass Mwall being ∞. Consequently, from the aforementioned formulas, the equivalent radius Req is equal to Rparticle, and the equivalent mass Meq is equal to Mparticle.

1.3. Governing equation of fluid mechanics

1.3.1. Computational fluid dynamics governing equations

According to the continuity equation, the net mass flowing out of a microelement per unit time is equal to the decrease in the mass of the microelement during that time.

$$\frac{\partial\rho}{\partial\text{t}} + \nabla\cdot(\rho V) = 0 \tag{14}$$

Where, is the Hamiltonian operator.

$$\nabla = \frac{\partial\text{i}}{\partial\text{x}} + \frac{\partial\text{j}}{\partial\text{y}} + \frac{\partial\text{k}}{\partial\text{z}} \tag{15}$$

$$\frac{\partial\rho}{\partial\text{t}} + \frac{\partial(\rho\text{u})}{\partial\text{x}} + \frac{\partial(\rho\text{v})}{\partial\text{y}} + \frac{\partial(\rho\text{w})}{\partial\text{z}} = 0 \tag{16}$$

According to the momentum equation, the rate of momentum change in a fluid microelement is equal to the sum of the rate of change in the momentum entering or leaving the surface of the control volume and various forces acting on the fluid microelement.

$$\frac{\partial(\rho u)}{\partial t}+\nabla\cdot(\rho uv)=-\frac{\partial p}{\partial x}+\frac{\partial \tau_{xx}}{\partial x}+\frac{\partial \tau_{yx}}{\partial y}+\frac{\partial \tau_{zx}}{\partial z}+\rho f_x$$

$$\frac{\partial(\rho v)}{\partial t}+\nabla\cdot(\rho vV)=-\frac{\partial p}{\partial y}+\frac{\partial \tau_{xy}}{\partial x}+\frac{\partial \tau_{yy}}{\partial y}+\frac{\partial \tau_{zy}}{\partial z}+\rho f_y \quad (17)$$

$$\frac{\partial(\rho w)}{\partial t}+\nabla\cdot(\rho wV)=-\frac{\partial p}{\partial z}+\frac{\partial \tau_{zx}}{\partial x}+\frac{\partial \tau_{zy}}{\partial y}+\frac{\partial \tau_{zz}}{\partial z}+\rho f_z$$

where $V = (u, v, w)$ represents the momentum conservation equation in the x-direction, y-direction, and z-direction, respectively; f is the volume force acting on the microelement; τ is the stress tensor; and p is the pressure acting on the microelement.

1.4. CFD-DEM coupling process

The CFD-DEM coupling process is as follows: 1) Establish a computational model, and provide the initial flow field, initial particle position, and initial particle velocity; 2) Use the DEM solver to calculate the various forces acting on particles, solve the particle momentum equation, and update the position and velocity of each particle; 3) After completing the DEM cycle, calculate the fluid particle interaction forces in the CFD grid cells and transfer them to the CFD cycle; 4) Solve the fluid momentum equation and continuity control equation to obtain the fluid velocity and pressure fields; 5) After the flow field converges, calculate the fluid force acting on the particles and replace it with the DEM solver; 6) CFD-DEM cycle calculation until the calculation end time is reached.

2. Ship–Ice model

2.1. Hull model

The geometric parameters of the *Xuelong* 2 hull are presented in Table 1.

A scale ratio of 1:40 was selected for the hull model with consideration of the computing power available in this study and the experimental data. Fig. 2 presents the geometric model of this hull.

Because of the hull's symmetry, only half of the hull was modeled. The size of the adopted computational domain (length × width × height) was 32 m × 10 m × 12 m. For time step convergence analysis. Firstly, perform a time step convergence analysis. Three different time steps were selected for analysis, and the specific values of the time steps and their corresponding water resistance are shown in Table 2. When the time steps are 0.01s and 0.05s, the calculated results are closer. Taking into account the accuracy of the simulation results and the

Table 1. Key parameters of the Xuelong 2 icebreaker.

T	Waterline length/m	Waterline width/m	Draft/m	Incidence angle of water plane/(°)
Full scale	116	22	7.8	3
Scale model	2.9	0.55	0.195	34

Source: Compiled by authors.

Fig. 1. China's polar icebreaker Xuelong 2 sailing in Antarctica. Source: the Internet.

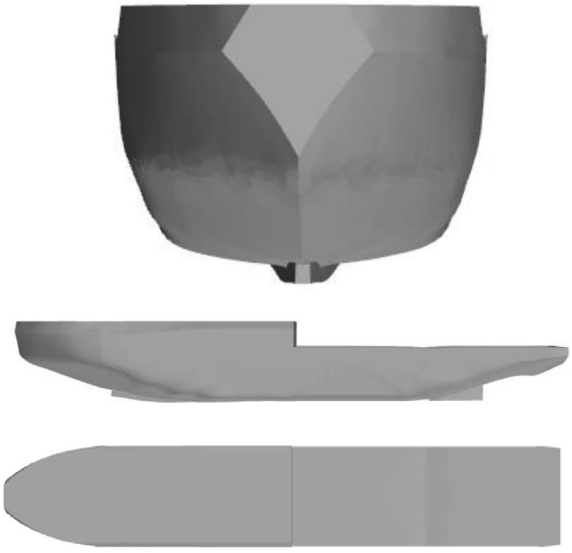

Fig. 2. Three views of the Xuelong 2 hull. Source: By authors.

Table 2. Convergence analysis for the Xuelong 2 time step.

Time step situation	Time step(S)	Water resistance
Time step 1	0.01	1.351N
Time step 2	0.05	1.339N
Time step 3	0.1	1.296N

efficiency of the calculation, time step 2, i.e. time step 0.0s, was selected for calculation.

Next, three different sizes of grids were used for grid convergence analysis. The specific values of the number of grids and their corresponding water resistance are shown in Table 3.

Increasing the number of grids had a strong effect on water resistance for Grid 3 and Grid 2 but a weak effect for Grid 2 and Grid 1. To obtain accurate simulation results with efficient calculations, Grid 2 was selected.

Fig. 3 shows the grid scene when Snow Dragon 2 selects Grid 2.

2.2. Settings of the ice element model

The numerical simulation software used in this study is STAR-CCM+,In this simulation, the physical model selected alternative implicit unsteady, Euler multiphase, fluid domain volume (VOF), K-Epsilon turbulence, gravity, cell mass correction and VOF wave,the overall process is as follows: geometric modeling, defining region layout, region meshing, defining physical model, post-processing settings, running simulation, and analyzing data results. In this case, Lagrangian multiphase is used to define ice floes and multiphase interaction is used to define the force between ice and ice, ship and water.

Based on the structural strength "Xuelong 2" and the LAN-Swedish Ice Scale Specification (FSICR), with IA Super The ice condition under the ice level is numerical, and the ice thickness is set as 0.6m This was done in line with the similarity criterion of Froude and Cauchy. Please, see Table 4 for the discrete-element model of floating ice parameters for the study's numerical simulation; and its cylindrical particles.

In the simulation, the ice floe cells were assumed to be unbreakable. The DEM module for the hull design was therefore a rigid wall.

Table 3. Convergence analysis for the Xuelong 2 grid.

Grid situation	Number of grids	Water resistance
Grid 1	6.8M	1.345N
Grid 2	3.8M	1.342N
Grid 3	1.77M	1.306N

Source: Compiled by authors.

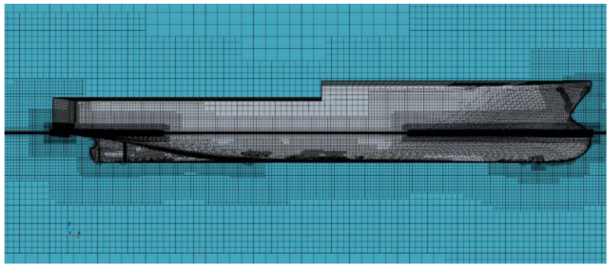

Fig. 3. Grid scene for Grid 2. Source: By authors.

Figs. 1 and 4 show *Xuelong 2* sailing in a polar ice waterway. Each ice floe has a different area, and the ice floes are randomly distributed [30]. According to relevant statistical data [31]. The floating ice area obeys the Log-normal distribution function, and the Log-normal distribution function is used to model the natural phenomena in the floating ice area, as shown in Fig. 5.

MATLAB was used to generate a random ice particle array that included the center and radius of each ice floe. The obtained results were then imported into STAR-CCM + for further analysis.

First, the boundary and radius of a circle were randomly determined. A function was used to generate a random point as the center of the circle. A new center point and radius were then randomly generated within a certain range of the previous point. This process was continued iteratively until the ice coverage requirement was met. Through this method, the density of floating ice can be controlled. Fig. 6 presents an illustration of a generated floating ice array,.its horizontal coordinate is the length of the floating ice channel along the ship's length, and the vertical coordinate is the length of the floating ice channel along the ship's width; and Fig. 7 presents the distribution of the areas of the generated floating ice. Both figures were generated in accordance with a log-normal distribution. Moreover, the speed of each ice particle and block was set to match the water flow rate (i.e., the current). Therefore, the ice array flowed toward the ship with the current.

After the entire floating ice array has flowed through the initial position used to generate it, a new floating-ice array can be generated at the same position (Fig. 8). By repeating this process, the simulated ship can always sail in the floe ice area despite the limited computational domain. This method considerably reduces the computational cost of the simulation.

3. Analysis and comparison with ship model test results

The simulation results of the present study were compared with the results of a ship–ice collision

Table 4. Parameters of the discrete-element model of floating ice.

Items	thickness/m	Young's modulus/Pa	Poisson's ratio	floating ice radius/m	Dynamic friction coefficient between ice and ship hull
Value	0.015	7.4×10^9	0.3	0.2–0.5	0.1

Source: Compiled by authors.

Fig. 4. Xuelong 2 in an ice channel. Source: By internet.

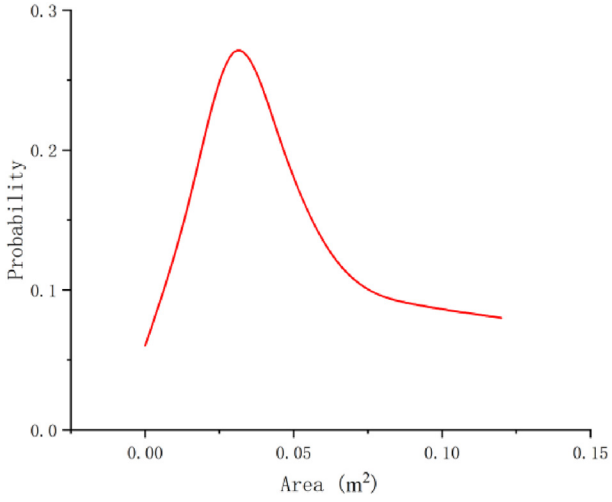

Fig. 5. Log-normal distribution of floe ice particles with different sizes. Source: By authors.

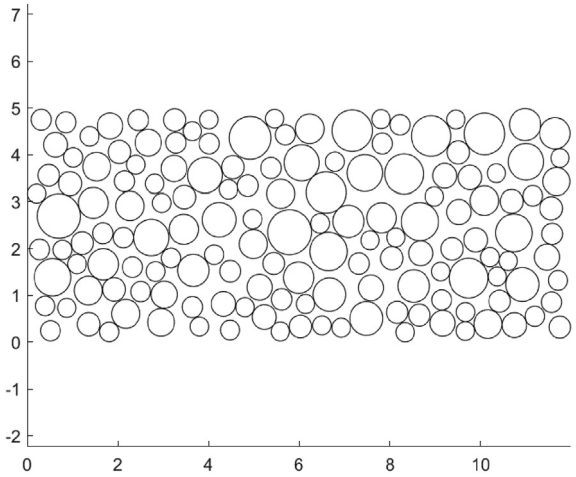

Fig. 6. Ice floe array with 60 % ice coverage. Source: By authors.

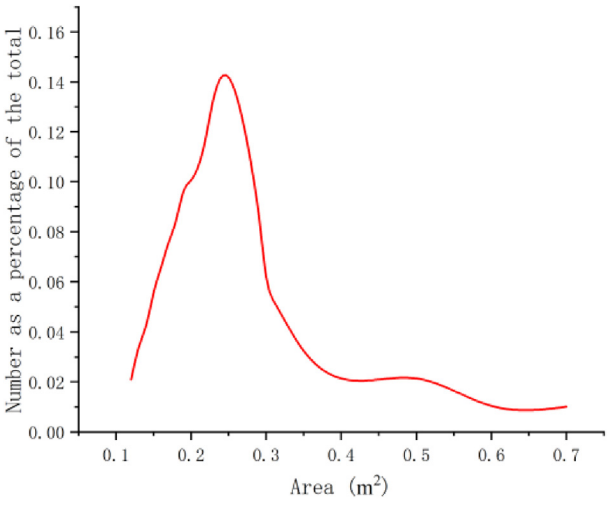

Fig. 7. Distribution of the areas of the generated floating ice. Source: By authors.

model experiment conducted in the Ice Mechanics and Engineering Laboratory of Tianjin University, China. This experiment was aimed at assessing the collision load during a ship–ice collision and the ice resistance of the ship. The ship model used in the aforementioned experiment a) comprised the hull lines of *Xuelong 2*, b) had a geometric scale ratio of 1:40, c) and had a speed of 0.553 m/s (consistent with the parameters of the numerical simulation model used in this study). Fig. 9 presents a photograph of the testing of the aforementioned ship model in the laboratory.

In collision simulation, the maximum force in the time history is selected as the characteristic resistance of the collision event. Table 5 shows the average resistance and characteristic resistance

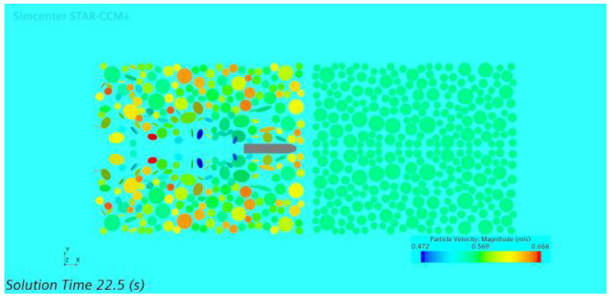

Fig. 8. Continuous generation of floating ice arrays. Source: By authors.

Fig. 9. Lab model test of Xuelong 2. Source: By authors.

Table 5. Ice resistance obtained from ship model experiments and numerical simulations.

	average resistance	characteristic resistance
ship model experiments	1.21 MN	12.97 MN
numerical simulations	1.09 MN	13.98 MN

obtained from ship model experiments and numerical simulations.

The average resistance of the numerical simulation is 1.09 MN, and the average resistance of the ship model test is 1.21 MN. The error is 9.1 %, so the numerical simulation results are in good agreement with the ship model test results.

In the calculation of collision load in the IACS specification, the influence of different impact positions on the ice load is considered: the hull head region is divided into four equal length subregions along the longitudinal direction, and then the middle position of each subregion is taken as the impact point, as shown in Fig. 10.

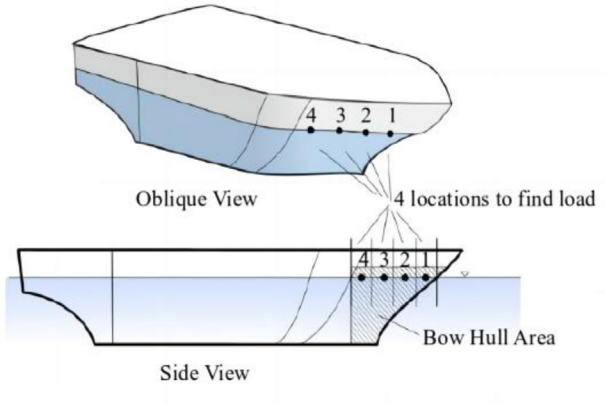

Fig. 10. A Schematic representation of the different impact locations. Source: By authors.

When the No.1 collision position is selected in this test, because when the collision position is set near the first column, the time course of the collision is fully developed and has a good application value for load assessment.

According to the IACS code, we can obtain the characteristic resistance Ft. Ft is 15.92 MN.Obtained results of the standard resistance Ft serving as the standard value, the test resistance Fm, and the characteristic resistance Fs from the numerical simulation were compared to ascertain the optimal ratio of characteristic resistance. As found in Table 6.

By comparison, the simulated resistance and the test resistance results were both recorded as smaller than the standard resistance ratio. It was also observed that the simulated characteristic resistance result was in good agreement with the ship model test characteristic resistance which met the requirement of regulation. From the above analysis, the numerical simulation of this study indicates that the ice load evaluation requirements were met.

4. Numerical calculations and analysis of the results

Fig. 11 shows a typical moment at a speed of 0.553 m/s with an ice coverage of 40 %,50 %,and 60 %.A part of the floating ice will collide with the bow of the ship when it flows to the ship. At this time, the floating ice will undergo displacement, overturn, increase in speed, and collide with other floating ice thereby resulting in a chain reaction. Following this chain reaction, friction is created from other ice floes which collide with some part of the hull. In effect, ice will be concentrated on both sides of the hull due to the crushing and colliding reaction of the ice floes located at the bow part.

4.1. Analysis of the numerical simulation results

This simulation considered the effects of different ice coverage with it associated speeds on ice resistance. Adherence to IACS technical specification, the design speed of the PC3 level was set to 3.5 m/s. Concurrently, three sets of speed conditions (thus, 90 %, 100 %, and 120 %) of the standard design speed (thus, 3.15 m/s, 3.50 m/s and 4.20 m/s) at the prototype scale were set respectively. More so,

Table 6. Ratios of the three characteristic resistances.

F_S/MN	F_M/MN	F_t/MN
0.88	0.81	1.00

Source: Compiled by authors.

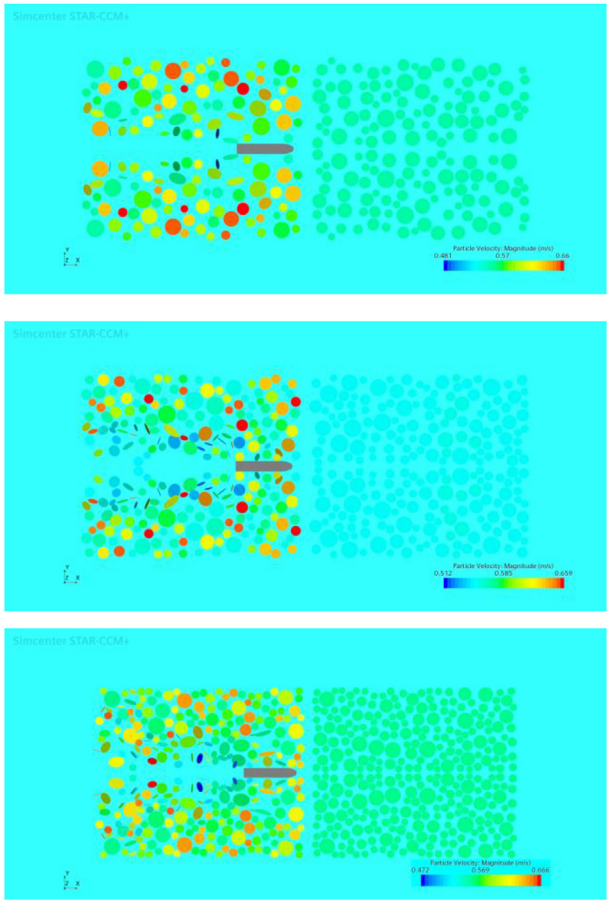

Fig. 11. Ship collision with ice floes at a speed of 0.553 m/s and ice coverage of 40 %,50 %,and 60 %. Source: By authors.

following the similarity criterion of Froude and Cauchy, the simulation velocities were set to 0.498 m/s, 0.553 m/s, and 0.664 m/s under the conditions of 40 %, 50 % and 60 % ice coverage respectively. Figs. 12–14 illustrates the above nine working conditions for the ice resistance simulation.

The mean resistance is the key factor that determines the endurance of an icebreaker. The mean resistance was calculated from the resistance curves obtained for each speed and ice coverage ratio. Moreover, the variations in the mean resistance with the ice coverage ratio at various speeds were obtained (Table 7 and Fig. 15).

Table 7 and Fig. 15 indicate that the ice coverage and ship speed considerably affected the ice resistance of the ship. Fig. 15 reveals that the average resistance value was positively correlated with the ice coverage and ship speed.

Further tests based on the aforementioned initial results were then performed. The resistance value obtained for a speed of 0.498 m/s with an ice coverage rate of 40 % was selected as the baseline value and compared with the mean resistance values for the other cases. The results are presented in Table 8.

The following conclusions are obtained from Table 8:

(1) At a higher ice coverage, the mean resistance value increased to a greater extent as the vessel speed increased.
(2) At a higher vessel speed, the mean resistance increased to a greater extent as the ice coverage increased

4.2. Comparison with the results obtained using an empirical formula

Using DuBrovin et al. [32] empirical formula proposed for calculating ice resistance, we compared the study's simulated data obtained with the average resistance value. See Equation (18) for empirical formula employed.

$$R_{ice} = p_1 A + p_2 \Phi F_{n^n} \tag{18}$$

where R_{ice} is the pure ice resistance of the icebreaker; P_1 and P_2 are empirical coefficients that depend on the ice coverage and channel width, respectively; F_n is the Froude number; and n is a dynamic coefficient that depends on the hull shape. The parameters A and Φ are defined as follows:

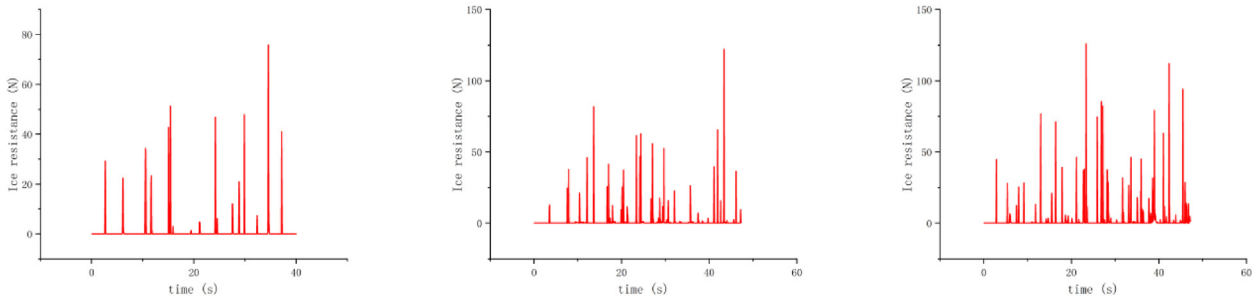

Fig. 12. Ice resistance for a ship speed of 0.498 m/s under an ice coverage of 40 %, 50 %, and 60 %. Source: By authors.

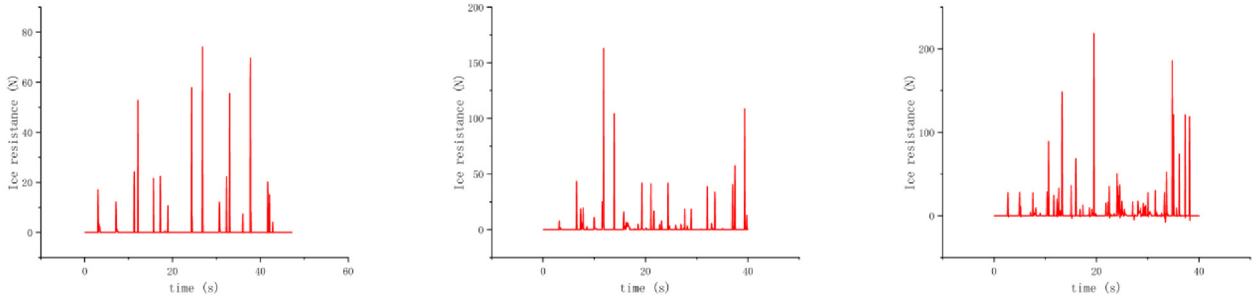

Fig. 13. Ice resistance for a ship speed of 0.553 m/s under an ice coverage of 40 %, 50 %, and 60 %. Source: By authors.

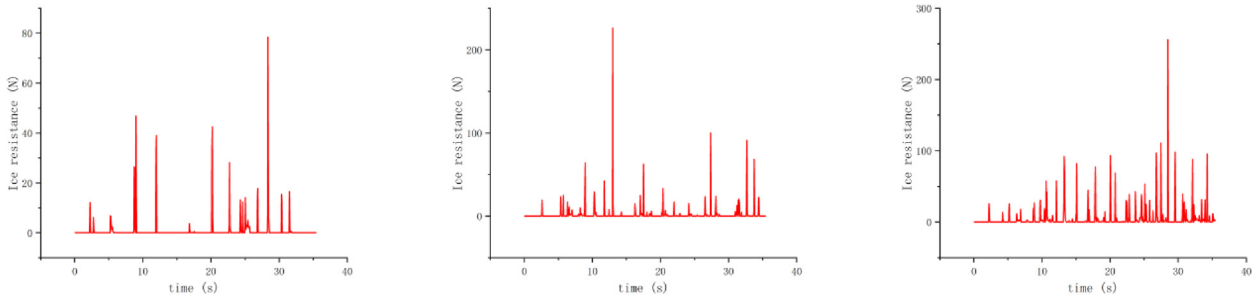

Fig. 14. Ice resistance for a ship speed of 0.664 m/s under an ice coverage of 40 %, 50 %, and 60 %. Source: By authors.

$$A=\frac{1}{4}B^2\sqrt{rh_{ice}}\rho_{ice}\left(1+2\frac{L}{B}f_0\alpha_H\right) \tag{19}$$

$$\Phi=rh_{ice}\rho_{ice}B\left[f_0+\tan\alpha_0\left(\alpha_H+\frac{L}{B}\tan\alpha_0\right)\right] \tag{20}$$

where ρ_{ice} is the density of the ice, r is the range of the floating ice, h_{ice} is the thickness of the ice, B is the width of the ship, L is the length of the ship, f_0 is the coefficient of friction between the ice and the hull, and α_0 and α_H indicate the angle when the edge of the floating ice collides with the ship on the waterline surface and the ship's fore body prismatic coefficient, respectively.

Applying the empirical formula calculation with the mean value of resistance under different ice coverage rates and speeds, we obtained results shown in Table 9. More so, the mean resistance calculated by the empirical formula was compared with the numerical simulation results, and errors was obtained in the following text.

The error was calculated as the mean square error (MSE) for groups of data with a given ice coverage or speed. For an ice coverage of 40 %, 50 %, and 60 %, the errors were 1.205, 0.9102, and 0.6327, respectively. For speeds of 0.498, 0.553, and 0.664 m/s, the errors

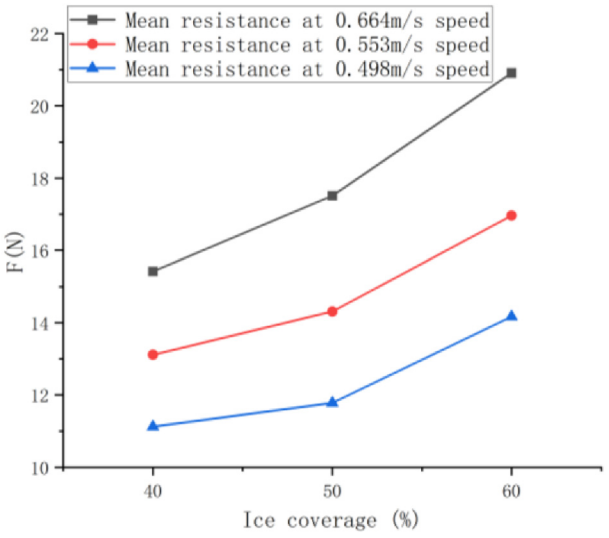

Fig. 15. Plot of mean resistance versus ice coverage for various speeds. Source: By authors.

Table 7. Mean ice resistance values

Ice Coverage	v = 0.498 m/s	v = 0.553 m/s	v = 0.664 m/s
40 %	11.12N	13.11N	15.42N
50 %	11.78N	14.31N	17.51N
60 %	14.17N	16.96N	20.91N

Source: Compiled by authors.

Table 8. Normalized ice resistance.

Ice coverage	v = 0.498 m/s	v = 0.553 m/s	v = 0.664 m/s
40 %	1	1.18	1.39
50 %	1.06	1.29	1.57
60 %	1.27	1.53	1.88

Source: Compiled by authors.

Table 9. Empirically calculated mean resistance values

Ice coverage	v = 0.498 m/s	v = 0.553 m/s	v = 0.664 m/s
40 %	12.24N	14.25N	16.45N
50 %	12.98N	15.40N	17.83N
60 %	15.04N	17.74N	21.64N

Source: Compiled by authors.

were 1.1504, 1.032, and 0.5654, respectively. The MSE can range from 0 to infinity; smaller values indicate a smaller error between the actual value and the predicted value. The aforementioned results suggest that the higher were the speed and ice coverage, the more consistent were the simulated and calculated mean ice resistance values.

The MSE calculation formula is shown in Equation (18).

$$\frac{1}{n}\sum_{t=1}^{n}\left(y_t - y_{tp}\right)^2 \tag{21}$$

where y_t is the numerical value, y_{tp} is empirical value, and n is the number of experiments.

5. Conclusion

The sailing process of *Xuelong 2* in polar ice floes was simulated and modeled in a laboratory setting for better understanding the effect of collisions between ice floes and ships. The sailing of *Xuelong 2* was modeled for different ice coverages and speeds, and the results revealed that both of these factors considerably affected the ship's ice resistance. The conclusions of this study are as follows:

(1) An increase in the vessel speed or ice coverage caused an increase in the resistance.
(2) The simulated results and the results calculated using Du Brovin's empirical formula were consistent. The error was smaller at higher ice coverage and vehicle speeds.
(3) The simulated and model ice resistance were in good agreement and substantially lower than the icebreaking standard. Therefore, the modeled ship met the ice load assessment requirements.

In the simulations performed in this study, only the ice resistance in the direction of the ship's length was analyzed. Moreover, the deformation and crushing of the floating ice were ignored. These limitations can be addressed in a follow-up study.

References

[1] He Yanping, Ren Yupei, Liu Yadong. Analysis and realization of the influence of sea ice flexural strength on ice resistance in numerical simulation of icebreaking by icebreaker. Ocean Eng 2023;273:1139953.
[2] Thomson J, Ackley S, Girard-Ardhuin F, Ardhuin F, Babanin A, Boutin G, et al. Overview of the arctic sea state and boundary layer physics program. J Geophys Res Oceans 2018;123(12):8674−87.
[3] Xuhao Gang, Tian Yukui, Ji Shaopeng, et al. Progress in Numerical Research on Ice Resistance of Ships Navigation in Ice Regions. Ship Eng 2020;42(9):6−13.
[4] Huang Luofeng, Tuhkuri Jukka, Igrec Bojan, Li Minghao. Ship resistance when operating in floating ice floes: A combined CFD&DEM approach. Marine Struct 2020;74:102817.
[5] Alberello A, Onorato M, Bennetts L, Vichi M, Eayrs C, MacHutchon K, Toffoli A. Brief communication: pancake ice floe size distribution during the winter expansion of the Arctic marginal ice zone. Cryosphere 2019;13:41−8.
[6] Lu W, Lubbad R, Serré N, et al. A theoretical model investigation of ice and wide sloping structure interactions[C]// 22nd Intl. Conf. on Port and Ocean Eng. Under Arctic Conditions. Espoo, Finland; 2013. p. 9−13.
[7] Yue Hong, Wu Xiaofeng, Zhao Yuxin. Development Status and Development Trends of Polar Ships. China Shipbuilding Inspect 2020;(7):58−64.
[8] Yulmetov R, Løset S. Validation of a numerical model for iceberg towing in broken ice. Cold Reg Sci Technol 2017;138:36−45.
[9] Yulmetov R, Lubbad R, Løset S. Planar multi-body model of iceberg free drift and towing in broken ice. Cold Reg Sci Technol 2016;121:154−66.
[10] Cundall PA. A computer model for simulating progressive large scale movements in blocky rock system. Proc Int Sympos Rock Fract 1971:1−8.
[11] Strack ODL, Cundall PA. The distinct element method as a tool for research in granular media，Part 1.Report to the National Science Foundation, Minnesota. University of Minnesota; 1978.
[12] Hansen EH, Løsetb S. Modelling floating offshore units moored in broken ice: comparing simulations with ice tank tests. Cold Reg Sci Technol 1999;29(2):107−19.
[13] Karulin EB, Karulina MM. Numerical and physical simulations of moored tanker behaviour. Ships Offshore Struct 2011;6(3):179−84.
[14] Lau M, Lawrence KP, Rothenburg L. Discrete element analysis of ice loads on ships and structures. Ships Offshore Struct 2011;6(3):211−21.
[15] Konno A, Saitoh O, Watanabe Y. Numerical investigation of effect of channel condition against ships resistance in brash ice channels[C]. In: Proc - Int Conf Port Ocean Eng under Arct Cond; 2011. POAC11-037).
[16] Xue Yanzhuo, Liu Renwei, Wang Qing, et al. Application Progress and Prospects of Near Field Dynamics in Ships and Marine Structures in Ice Regions. Chinese J Ship Res 2021;16(5):1−15.
[17] Kim HS, Ryu CH, Park KD, et al. Development of estimation system of ice resistance with surface information of hull form. Ocean Eng 2014;92:12−9.
[18] Kim MC, Lee WJ, Shin YJ. Comparative study on the resistance performance of an icebreaking cargo vessel according to the variation of waterline angles in pack ice conditions. Int J Nav Archit Ocean Eng 2014;6(4):876−93.
[19] Kim Jeong-Hwan, Kim Yooil, Lu Wenjun. Prediction of ice resistance for ice-going ships in level ice using artificial neural network technique. Ocean Eng 2020:217.
[20] Zhao Weidong, JohanLe ra Bernt, EkaterinaKim. A Probabilistic Framework for the Fatigue Damage Assessment of Ships Navigating through Level Ice Fields. Appl Ocean Res 2021;111(2021):102624.
[21] Yuan Dongfang, Wang Shuoren, Chen Qingman. etc The polar application of the "Snow Dragon 2" long column sampler. Polar Res 2021;33(3):459−68.
[22] Chen Qingman, Wang Shuoren. Zhao Yanping Design and Application of the Moon Pond System on the "Xuelong 2" Polar Expedition Ship. Chinese Ship Res 2021;16(5):30−8.

[23] Luo W, Jiang D, Wu T, Guo C, Wang C, Deng R, Dai S. Numerical simulation of an ice-strengthened bulk carrier in brash ice channel. Ocean Eng 2020;196:106830.
[24] Tang X, Zou M, Zou Z, Li Z, Zou L. A parametric study on the ice resistance of a ship sailing in pack ice based on CFD-DEM method. Ocean Eng 2022;265:112563. 2022.
[25] Zhang J, Zhang Y, Shang Y, Jin Q, Zhang L. CFD-DEM based full-scale ship-ice interaction research under FSICR ice condition in restricted brash ice channel. Cold Reg Sci Technol 2022;194:103454.
[26] Georgiev P, Garbatov Y. Multipurpose vessel fleet for short black sea shipping through multimodal transport corridors. Brodogradnja 2021;72(4):79−101.
[27] Norozi HR, Za Rghami R, So TR. Couple CFD-DEM Modeling: Formulation, Implementation and Application to Multiphase Flows. Wiley Online Lib 2021;165(2):752−70.
[28] Han Yuxin. Research on damage stability of arctic navigation ships. Dalian University of Technology; 2021. p. 001115.
[29] Walton K. The effective elastic moduli of a random packing of spheres. J Mech Phys Solid 1987;35(2):213−26.
[30] Guo C, Xie C, Zhang J, Wang S, Zhao D. Experimental investigation of the resistance performance and heave and pitch motions of ice-going container ship under pack ice conditions. China Ocean Eng 2018;32:169−78.
[31] Chang Xie. Experimental study on the resistance performance of ships in ice regions under broken ice conditions [D]. Harbin University of Engineering; 2015.
[32] Dubrovin OV. Calculation of broken ice resistance based on model testing[R]. Translated: ALEKSANDROV M, MOOR R. The Department of Navel Architecture and Marine Engineering, University of Michigan of Engineering; 1970.